Analysis of Temporal Shear Stress Gradients During the Onset Phase of Flow Over a Backward-Facing Step

Mark A. Haidekker
Charles R. White
John A. Frangos

University of California, San Diego,
Department of Bioengineering,
La Jolla, CA 92092-0412

Endothelial cells in blood vessels are exposed to blood flow and thus fluid shear stress. In arterial bifurcations and stenoses, disturbed flow causes zones of recirculation and stagnation, which are associated with both spatial and temporal gradients of shear stress. Such gradients have been linked to the generation of atherosclerotic plaques. For in-vitro studies of endothelial cell responses, the sudden-expansion flow chamber has been widely used and described. A two-dimensional numerical simulation of the onset phase of flow through the chamber was performed. The wall shear stress action on the bottom plate was computed as a function of time and distance from the sudden expansion. The results showed that depending on the time for the flow to be established, significant temporal gradients occurred close to the second stagnation point of flow. Slowly ramping the flow over 15 s instead of 200 ms reduces the temporal gradients by a factor of 300, while spatial gradients are reduced by 23 percent. Thus, the effects of spatial and temporal gradients can be observed separately. In experiments on endothelial cells, disturbed flow stimulated cell proliferation only when flow onset was sudden. The spatial patterns of proliferation rate match the exposure to temporal gradients. This study provides information on the dynamics of spatial and temporal gradients to which the cells are exposed in a sudden-expansion flow chamber and relates them to changes in the onset phase of flow.
[DOI: 10.1115/1.1389460]

Introduction

The vascular endothelium is uniquely situated to act as the signal transduction interface between hemodynamic forces and the underlying smooth muscle. Many early events in the pathogenesis of atherosclerosis are linked, at least initially, to complex hemodynamic forces unique to atherosclerotic prone regions of the vasculature [1]. Flow characteristics such as flow separation, recirculation and reattachment, as it occurs close to arterial bifurcations, may directly contribute to the initiation of focal atherogenesis [2,3]. Conversely, steady laminar shear stress, as it occurs in non-curving regions of the vasculature, induces vasoprotective nitric oxide [4] and prostacyclin synthesis [5], and inhibits proatherosclerotic endothelial turn-over [6].

A number of studies have suggested that localized spatial gradients in shear stress can induce a proatherosclerotic endothelial cell proliferation-migration-loss cycle at the point of flow stagnation [2,3]. Activation of endothelial cell proliferation has been reported at sites with a spatial gradient between 4 and 8 Pa/m [7,8]. However, throughout each stage of the cardiac cycle, the change in flow rate and shear stress can also generate localized temporal gradients in shear stress. At sites of flow separation and flow reversal, such as anastomoses [9] or the human carotid artery [10], the endothelium is exposed to overlapping temporal and spatial gradients of shear stress. In cultured endothelial cells, transient temporal gradients in shear stress as short as 3 s in duration have been shown to stimulate the expression of PDGF-A and MCP-1 as well as activate the pro-mitogenic MAPkinase signalling pathway [11,12]. Furthermore, oscillating shear stress has been shown to coincide with sites of intimal thickening in the human aorta [13]. Clearly, spatial and temporal gradients overlap in atherosclerosis prone regions and must be separated in order to determine which of the two stimuli is the main cause of atherosclerotic plaque growth.

An established *in vitro* model used to simulate flow in bifurcating arterial regions is the backward-facing step flow chamber [14]. In this model, fluid flows from a narrow channel over a step expansion into a wider channel. The asymmetric expansion of the flow path leads to a separation of the flow. Close to the expansion step, there is a recirculating eddy with a flow direction against the main flow. Farther downstream, the flow reattaches and eventually re-establishes a unidirectional parabolic flow profile. At physiological Reynolds numbers, the flow is laminar in the entire chamber. In the backward-facing step flow chamber, endothelial cells exposed to the separated flow streams experience large spatial shear stress gradients, especially close to the second stagnation point. However, if the onset of flow is sudden in the backward-facing step flow chamber (i.e., rapid increase of the inflow velocity), the steady state of the flow requires several milliseconds to develop fully [15], subjecting the cells to a large temporal gradient of shear stress. Therefore, cells in the region of recirculating flow are exposed to both spatial and temporal gradients of shear simultaneously if the flow of the system is turned on instantaneously. The temporal gradient in the backward-facing step flow chamber can be effectively eliminated if the onset of flow is slowly ramped up. By comparing the effects of a sudden onset of flow (with both temporal and spatial gradients) with that of slowly ramped flow (where temporal gradients are close to zero), the purported proatherosclerotic effect of these two distinct mechanical stimuli effects can be separated.

For a better understanding of the magnitude of temporal shear stress gradients, numerical methods have been used in this study to elucidate time-dependent changes in fluid flow. Based on the initial observation of a relatively slow development of the eddy [15], flow simulations have been performed for different flow onset times and for different expansion ratios, focusing on the result-

Contributed by the Bioengineering Division for publication in the JOURNAL OF BIOMECHANICAL ENGINEERING. Manuscript received by the Bioengineering Division July 6, 2000; revised manuscript received April 17, 2001. Associate Editor: J. E. Moore, Jr.

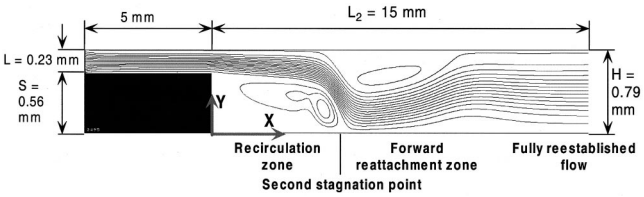

Fig. 1 Geometry of the backward-facing step flow chamber with the dimensions used in the computer simulation. The origin of the coordinate system is the lower right corner of the expansion step. In order to keep the grid size small, only the first 15 mm downstream of the expansion site were considered in the model, since the fully reattached parabolic-profile flow is established at that point. Also shown are the streamlines of the steady-state flow at Re=243 with the second stagnation point at 4.8 mm.

ing wall shear stress. Experiments were performed to verify the numerical results. In light of observations that localized elevations in endothelial cell turn-over is an early event in atherosclerotic plaque development [7], the spatial distribution of endothelial cell proliferation after exposure to time-dependent fluid flow was also determined.

Materials and Methods

Flow Chamber With Backward-Facing Step. The backward-facing step flow chamber used in this study was a modification of the chamber described by Truskey [14]. It consisted of a polycarbonate block with the inlet and outlet ports, two medical-grade silicone gaskets of a nominal thickness of 0.51 and 0.25 mm, and a glass slide. The flow channel was cut into the gaskets, 59.5 by 21 mm for the 0.25 mm gasket, and 53 by 21 mm for the 0.51 mm gasket. A vacuum applied to a third port in the polycarbonate block secured the components together. Micrometer measurements showed actual thicknesses of 0.56 mm for the thicker gasket (this is the actual step height S) and 0.23 mm for the thinner gasket (which is the inflow channel height L). The resulting outflow channel height was therefore 0.79 mm and the expansion ratio $(L+S)/L=3.4$. For the flow simulations, the height values $L=0.23$ mm (inflow) and $S=0.56$ mm (step height) were used. The origin of the coordinate system was located at the lower edge of the expansion point. The simulated channel extends 5 mm in negative x direction (before the sudden expansion), and 15 mm in positive x direction, after the sudden expansion. The main direction of the flow is positive in x. The geometry is depicted in Fig. 1.

Numerical Simulations of Flow. It has been observed that in a similar backward-facing step flow channel, the flow is homogeneous in the third dimension for about 80 percent of the width of the flow channel [14], and that the calculated values for the second stagnation point and shear stress do not significantly vary between a two-dimensional and a three-dimensional model. Also, the Reynolds numbers in this study have been found to be within a range of two dimensionality of the flow [16,17]. For this reason, a two-dimensional model was chosen. The governing equations, the momentum Eq. (1) and the continuity Eq. (2) for viscous, incompressible fluids, were solved numerically by employing a finite-element staggered grid discretization with a weighted combination of upwind and central differences.

$$\frac{\partial}{\partial t}\vec{u}+(\vec{u}\ \mathrm{grad})\vec{u}+\mathrm{grad}\,p=\frac{1}{\mathrm{Re}}\Delta\vec{u}+\vec{g} \tag{1}$$

$$\mathrm{div}\,\vec{u}=0 \tag{2}$$

In Eqs. (1) and (2), $\vec{u}=(u_x,u_y)$ is the velocity field, p is the pressure, and g the body forces, which in this case are neglected $(g=0)$. Normalization took place over the inflow channel height L and the variable average inflow velocity u_∞ so that the Reynolds number is defined as (3):

$$\mathrm{Re}=\frac{\rho}{\mu}u_\infty L \tag{3}$$

For the simulations with ramped flow, the spatial grid was made up of 600 by 100 nodes for a dimensional size of 20 by 0.79 mm, 15 mm for the length of the channel downstream of the expansion step. The detailed procedure has been described in [15], and the algorithm is outlined in the appendix.

For the simulation of ramped flow, the Reynolds number was increased linearly from $\mathrm{Re}_{\min}=10$ at $t=0$ to $\mathrm{Re}_{\max}=243$ at $t=t_{\mathrm{ramp}}$, and kept constant thereafter. For each discrete time step, the step size δt was chosen so that the stability condition (4) with $\kappa=0.5$ was satisfied, resulting in an adaptive stepsize algorithm:

$$\delta t\leq\kappa\cdot\min\left\{\frac{\mathrm{Re}}{2}\left(\frac{1}{\delta x^2}+\frac{1}{\delta y^2}\right)^{-1},\ \frac{\delta x}{|u_{x\max}|},\ \frac{\delta y}{|u_{y\max}|}\right\} \tag{4}$$

To verify the suitability of the selection of $\kappa=0.5$, a ramped-flow simulation ($t_{\mathrm{ramp}}=200$ ms) was performed for discrete values of $\kappa=0.9,0.8,\ldots,0.2$ and the resulting maximum shear stress and position of the second stagnation point were analyzed for convergence.

In regular time intervals, the wall shear stress was calculated for the momentary flow situation (Eq. (15)), which in its discrete form and observing the staggered grid geometry becomes Eq. (5):

$$\tau(x,t)=\mu\left.\frac{\partial u_x(x,y,t)}{\partial y}\right|_{y=0}=\frac{2U_x(x,\delta y,t)}{\delta y}\cdot\frac{\mu u_\infty}{L} \tag{5}$$

The shear stress $\tau(x,t)$ is recorded in dependency of the x position downstream from the sudden expansion point and the time. Using central differences, the temporal shear stress gradient (Eq. (6)) and the spatial shear stress gradient (Eq. (7)) were computed.

$$\dot{\tau}(x,t)=\frac{\partial\tau(x,t)}{\partial t}\approx\frac{\tau(x,t-\delta t)-\tau(x,t+\delta t)}{2\,\delta t} \tag{6}$$

$$\tau'(x,t)=\frac{\partial\tau(x,t)}{\partial x}\approx\frac{\tau(x+\delta x,t)-\tau(x-\delta x,t)}{2\,\delta x} \tag{7}$$

Along the bottom wall $(y=0)$, points exist where the flow stagnates $(u_x=u_y=0)$. The first stagnation point occurs at $x=0$. The second stagnation point occurs downstream of the recirculation eddy and is the site where the major spatial gradients have been reported. The position of the second stagnation point changes with the flow rate, and also changes with time until a steady state is reached.

Experiments With Endothelial Cells. The described backward-facing step chamber was used to expose human umbilical cord vein endothelial cells (HUVEC) to shear stress with different ramp times in order to determine the influence of spatial and temporal gradients on cell proliferation. Primary human umbilical vein endothelial cell (HUVEC) isolation was performed as previously described [18]. Dulbecco's modified Eagles's medium (DMEM, Irvine Scientific) supplemented with 2 percent heat-treated FBS (Hyclone), 0.5 U/ml penicillin, and 0.05 mg/ml streptomycin, was used as the perfusing medium for all experimental procedures. All flow chambers and accompanying apparatus were placed in an air curtain incubator and maintained at 37°C throughout the experiment. Time-matched sham controls (slides mounted on flow chambers without flow) and static controls (undisturbed slides in Petri dishes) were performed for all experimental groups. All experiments were conducted under sterile conditions. HUVEC were grown to confluence on glass slides within three days, attached to the flow chamber as described above, and then subjected to 4 hours of flow. One of two methods for the onset of flow were used: (1) sudden onset (the initiation of fully established flow at

3.5 ml/s, which corresponds to Re=243, within 200 ms); or (2) ramped onset (a smooth ramped increase in flow from 0 to 3.5 ml/s within 15 s). The continuous flow of media through the flow chamber was maintained with a constant hydrostatic pressure head flow loop apparatus [5]. Immediately following the completion of each specific flow profile, slides were removed from the flow chamber to be assayed for HUVEC proliferation as follows.

Proliferating HUVEC were identified by using a commercially available *in situ* monoclonal antibody kit for the detection of bromodeoxyuridine (BrdU) incorporation into cellular DNA during DNA synthesis (Boehringer Mannheim cat# 1296-736). Immediately after exposure to flow, slides were quickly removed from the chamber and incubated at 37°C in M199-BrdU (10 μmol/l BrdU) for 22 hours. Slides were fixed in 70 percent ethanol (in 50 mM glycine buffer, pH 2.0), and immuno-stained for BrdU incorporation. BrdU positive cells were visualized under a fluorescence microscope (Nikon Diaphot TMD). Proliferating cells were counted by eye within adjacent 40× high-power fields of view (HPF) along the centerline of each slide. Each HPF was divided into 1.1 mm sections extending 20.2 mm downstream from the expansion point. All reported values of n refer to the number of separate experiments from multiple primary HUVEC cultures. The results are presented as average ±SEM. For the data of each individual HPF the Kolmogorov–Smirnov test was used to verify that the distribution was Gaussian, and the t-test was performed to check for statistical significance (level of significance at $p<0.05$) of the difference between the sudden-onset proliferation rates and the ramped-onset proliferation rates.

Results

Validation of the Model. For the given geometry ($H=0.79$ mm, $S=0.56$ mm, $w=21$ mm, $L=H-S=0.23$ mm) and Re=243, the steady-state flow was calculated for grid sizes of 70×14, 150×28, 300×50, 600×100, and 1200×200 pixels. Figure 2 shows the highest shear stress found in the recirculation zone and in the forward reattachment zone in dependency of the grid size. Between the last two grid sizes analyzed, there was less than 3 percent difference. For all further simulations, a grid of 600×100 was selected since a higher resolution did not result in a relevant change of the flow and shear values. Based on this grid setting, the suitability of the chosen discrete time steps (Eq. (4)) was verified by performing a ramped-flow simulation with $t_{ramp}=200$ ms. The maximum shear stress in the recirculation zone and the position of the second stagnation point were compared for $\kappa=0.9,0.8,\ldots,0.2$. It can be seen in Fig. 2 that no significant change of both values occurs for $\kappa\leqslant 0.6$. For all further experiments, $\kappa=0.5$ was chosen. The discrete time steps computed using Eq. (4) were 32 μs (at the beginning of the simulation) to 11 μs (at $t>t_{ramp}=200$ ms).

Development of the Recirculating Flow. Due to inertia effects, tubing elasticity, and mechanical properties of the valve, the inflow velocity will increase in a monotonous, but not necessarily linear, fashion over a short period of time and then remain constant. In the video visualizations, this time was found to be 200 ms. In the model, the flow increase during the onset time was assumed to be linear. Figure 3 shows the simulated development of the flow in the flow chamber at various times. It can be seen that the development continues for about 100 ms after the inflow velocity reached its final value of 3.5 ml/s. The precise temporal behavior can be seen in Fig. 4, where the position of the second stagnation point is plotted over the elapsed simulation time. The wall shear stress at the bottom plate of the flow chamber also changes with time. Using Eq. (5), the wall shear stress $\tau(x,t)$ was computed as a function of a location and time. For the ramp time of 200 ms, this three-dimensional graph is shown in Fig. 5, its partial temporal derivative $\partial\tau(x,t)/\partial t$ in Fig. 6, and its partial spatial derivative in Fig. 7. In Fig. 5, the development of the recirculation eddy can be recognized as the development of the ridge. In panel *B* of Fig. 5, this corresponds to the development of the yellow/red zone (forward-directed flow) and the blue zone (recirculating flow) when going from the left to the right, i.e., advancing in time. The thin green zone (white arrow in Fig. 5) between the red and the blue area is the temporal development of the second stagnation point and corresponds to Fig. 4. Figure 6 shows the temporal derivative of the function in Fig. 5. As the system reaches a steady state, the temporal derivative vanishes (right side of the graphs). It can also be seen that during the onset phase, significant temporal gradients of shear stress also occur downstream of the second stagnation point (yellow zone above $X/S=8$). Likewise, Fig. 7 shows the partial derivative of the wall shear stress towards x. The highest spatial gradients can be observed close to the second stagnation point.

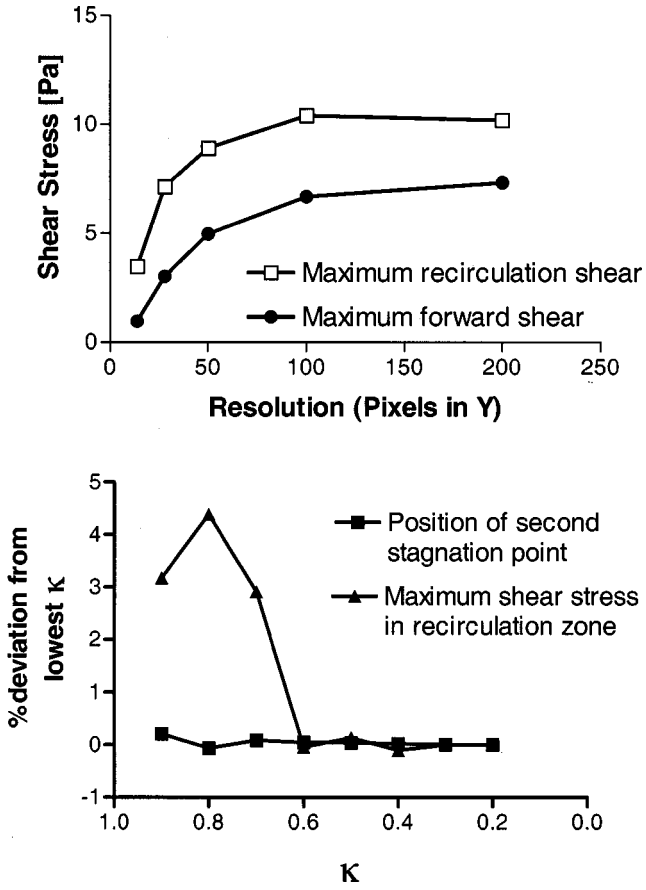

Fig. 2 Upper panel: Calculated changes of the highest shear stress values with increasing grid size. Resolutions of 70×14, 150×28, 300×50, 600×100, and 1200×200 grid nodes were chosen, and the steady-state flow at Re=243 computed. There is no significant change (less than 3 percent) between the two largest grid sizes. Lower panel: Different time step sizes (parameter κ in Eq. (4)) were used to verify the convergence of the discretization of the momentum equation. No significant changes were observed for $\kappa\leqslant 0.6$.

The magnitude of the temporal gradient strongly depends on the ramp time. The above-described simulation was performed for ramp times of 50, 100, 200, 500 ms, and for 1, 2, and 15 seconds. The resulting maximum temporal gradient that occurs within the recirculation zone is graphed in Fig. 8. A hyperbolical decay function, Eq. (8), can be fitted to the data points.

$$\dot{\tau}_{max}=A\cdot\frac{1}{t_{ramp}^{B}} \tag{8}$$

In Eq. (8), $\dot{\tau}_{max}$ is the predicted maximum value of the temporal shear stress gradient, t_{ramp} is the ramp time, and the constant A

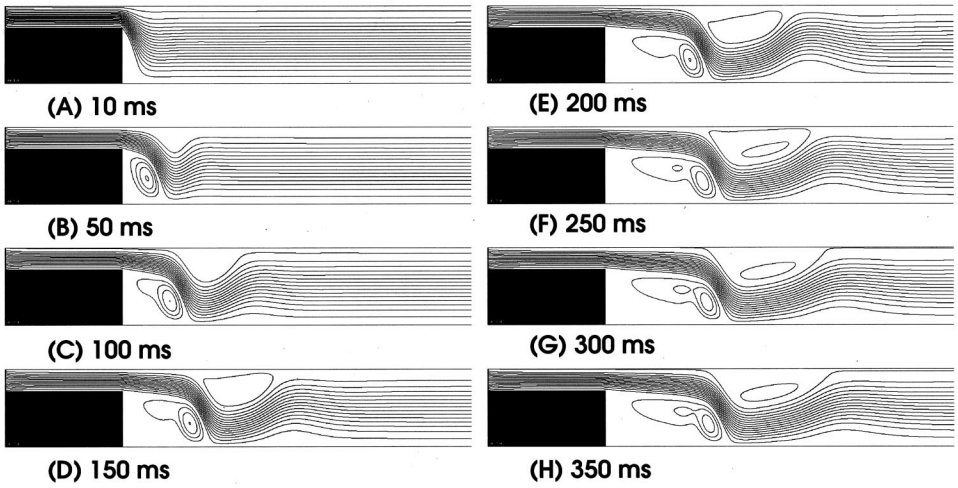

Fig. 3 Streamlines of the developing flow in the flow chamber during a simulated 200 ms linear onset phase of the inflow velocity. After 200 ms, the inflow velocity reaches its final values of 3.5 ml/s. A steady state is reached approximately 300 ms after the initial onset of flow. During the final 100 ms, the recirculation eddy keeps developing, although the flow rate is constant.

was determined from the empirical data by nonlinear regression. The constants were found as $A=221.5$ and $B=1.15$ with a regression coefficient of $R^2=0.999$. Due to the empirical nature of the curve fit, units for A are not given. In a similar way, the dependency of the maximum spatial gradients on the ramp time was computed and is shown in Fig. 9. It was found that an exponential decay showed a markedly better approximation of the data points than the hyperbolical curve fit used for the temporal gradients. Thus, the maximum spatial gradient (τ'_{max}) as a function of the ramp time t_{ramp} was empirically approximated according to Eq. (9):

$$\tau'_{max}=s\cdot\exp\left(-\frac{t_{ramp}}{K_t}\right)+P \tag{9}$$

The constants are $s=42.7$ kPa/m, $K_t=8.6$ ms, and $P=40.11$ kPa/m with a regression coefficient of $R^2=0.995$. While the temporal gradients vanish with $t_{ramp}\rightarrow\infty$, the maximum spatial gradients approach the finite limit P. Furthermore, the spatial gradients during sudden onset of flow ($t_{ramp}=200$ ms) are about 25 percent higher than in the slowly ramped case ($t_{ramp}=15$ s), while the temporal gradients differ by a factor of 300 when original data points are used (488 Pa/s for $t_{ramp}=200$ ms and 1.66 Pa/s for ($t_{ramp}=15$ s) or a factor of 145 when the curve fit (Eq. (8)) is being used.

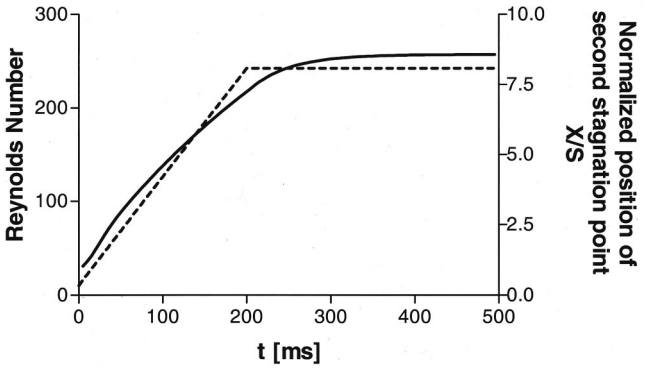

Fig. 4 Development of the recirculation eddy in dependency of time. The Reynolds number is ramped linearly over 200 ms (dashed line). After 200 ms, when the inflow velocity is kept constant, the recirculation zone keeps increasing in size. At 300 ms, the position of the second stagnation point lies within 2 percent of its steady-state value, $X/S=8.6$, which corresponds to 4.8 mm downstream of the expansion site.

To determine the influence of the step geometry on the shape of the function $\tau(x, t)$, the maximum shear stress in the recirculation zone was determined in dependency of the expansion ratio at constant Reynolds numbers. Figure 10 shows the ratio of maximum shear stress to outflow shear stress for expansion ratios of 1:2, 1:2.27, 1:2.94, 1:3.33, and 1:3.58. An almost linear relationship between the data pairs was observed, which indicates that a higher expansion ratio amplifies the shear stress in the recirculation zone over the shear stress in the region of fully reattached flow.

Effect of Ramped Versus Sudden Onset of Flow in SEFC on HUVEC Proliferation. Figure 11 shows photomicrographs of two representative HUVEC monolayers after 4 hours' exposure to recirculating flow with sudden onset (200 ms) and ramped onset (15 s) of flow, respectively. Each white dot represents a proliferating cell (BrdU positive nucleus). The higher density of proliferating cells in the top panel can clearly be seen. Also, the density of proliferating cells is higher close to the second stagnation point where the highest shear stress gradients occur. While both cell populations were exposed to the same steady-state flow situation, the top panel was experiencing higher temporal gradients of shear stress, especially close to the second stagnation point. This suggests that the temporal gradients stimulate cell proliferation. The proliferation rate of cells exposed to high temporal gradients ($n=12$) and the proliferation rate of cells under slowly ramped flow conditions ($n=8$) in each contiguous HPF can be seen in Fig. 12. Also shown is the calculated total (time-integrated) exposure of the cells to temporal changes of fluid flow (Eq. (10)).

$$\tau_{total}(x)=\int_0^{\infty}\left|\frac{\partial\tau(x,t)}{\partial t}\right|dt \tag{10}$$

The increased proliferation rate under a sudden onset of flow is statistically significant in the HPF range from 2.2 to 7.7 mm. This range coincides with the downstream area where the highest exposure to temporal gradients of shear stress was calculated.

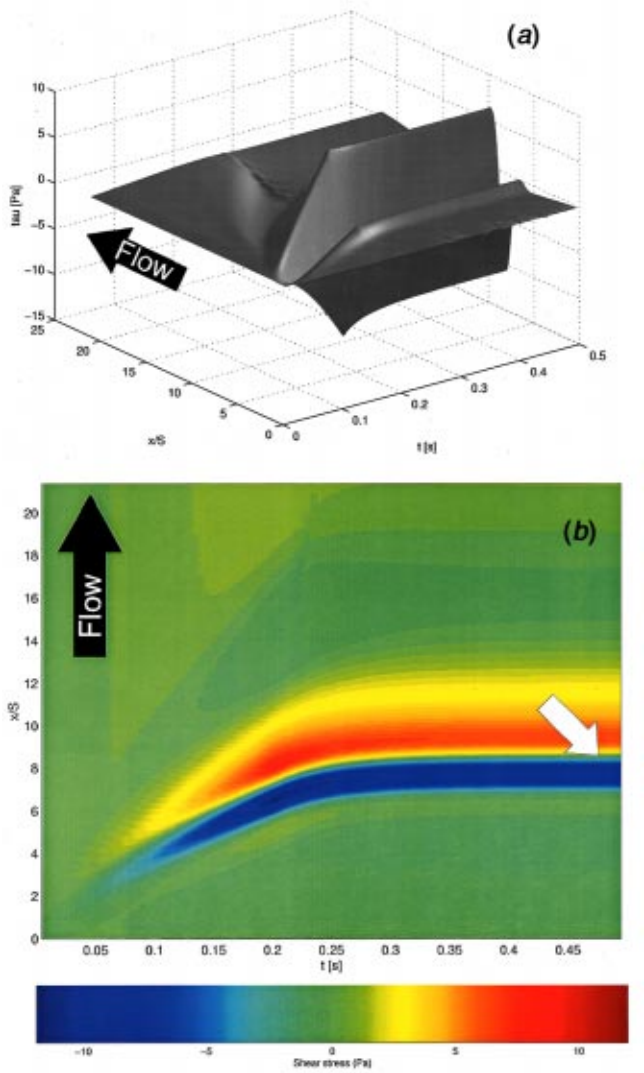

Fig. 5 Graphs of the bottom plate shear stress as a function of location and time, $\tau(x,t)$. The same function is shown as a three-dimensional graph (A) and a false-color contour plot (B) with yellow and red colors indicating the forward shear stress after the second stagnation point and blue colors indicating the recirculation zone. The final position of the second stagnation point is indicated by the white arrow. The onset phase of flow can easily be recognized by the rise of shear stress and the movement of the second stagnation point: Moving forward in time is equivalent to moving to the right. The sudden-expansion site is represented by the lower edge of the right graph or the right edge moving towards the right background in the left graph. The flow direction is indicated by black arrows. [Subscribers to the JOURNAL OF BIOMECHANICAL ENGINEERING may access Figs. 5(B), 6(B), and 7(B) in color on-line at http://ojps.aip.org/ASMEJournals/Biomechanical.]

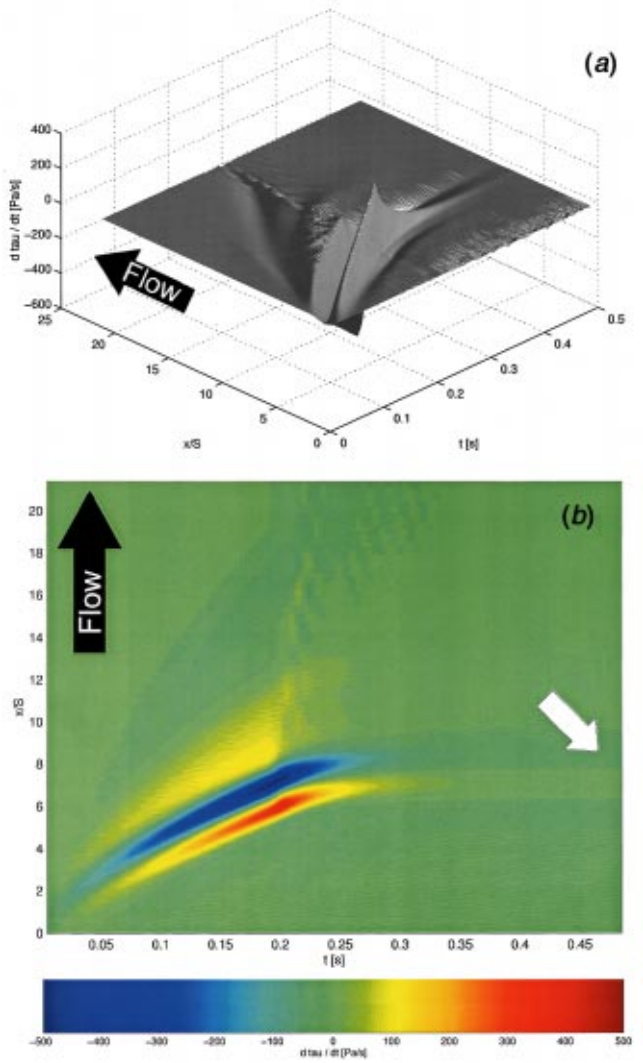

Fig. 6 Temporal partial derivative of the function shown in Fig. 5. As in Fig. 5, the same data are presented as a three-dimensional graph and a two-dimensional false-color contour plot. The graphs show that the highest temporal gradient of the shear stress occurs at the time the ramping ends. The system then reaches a steady state after approximately 300 to 350 ms, after which the temporal gradient remains zero. The zone exposed to the highest temporal gradients is located slightly upstream of the second stagnation point.

Discussion

Increased endothelial turnover in regions of recirculating flow has long been implicated in the early process of atherogenesis [7,8,19]. The anatomically localized patterns of the earliest lesions of atherosclerosis strongly suggest that complex in vivo flow characteristics such as flow separation, recirculation, and reattachment, oscillations in shear stress, and large spatial gradients may directly contribute to the initiation of focal atherogenesis [2,3]. With the development of the backward-facing step flow chamber model that simulates in vivo spatial patterns of flow separation, recirculation, and reattachment [8,14], a number of investigators have experimentally demonstrated the pro-atherosclerotic effect of flow recirculation on endothelial cells [8,14,20,21]. Despite studies that link pro-mitogenic MAPkinase activation, and PDGF-A and MCP-1 gene induction, to temporal gradients in shear stress [11,12], to date, the induction of these atherogenic phenotypes has been attributed primarily to spatial gradients of shear stress.

The same sites that exhibit disturbed flow patterns, such as the carotid bifurcation or blood vessels with stenosis, also expose the endothelium to temporal gradients due to changing flow rates over the cardiac cycle [10,22]. Measuring maximum slopes in published graphs of $\tau(t)$ yields values of 23 Pa/s [22] to 42 Pa/s [10] for the outer wall of the bifurcation and 86 Pa/s [10] for the inner wall. In the abdominal aorta, values between 50 and 80 Pa/s were obtained [23]. The SEFC geometry used in this study does not simulate physiological conditions. The geometry of the SEFC was designed to amplify temporal and spatial flow patterns within a region of recirculating flow. As employed in this study, the SEFC was used to differentiate and mathematically model the temporal gradients in shear from that of spatial gradients. In contrast to in

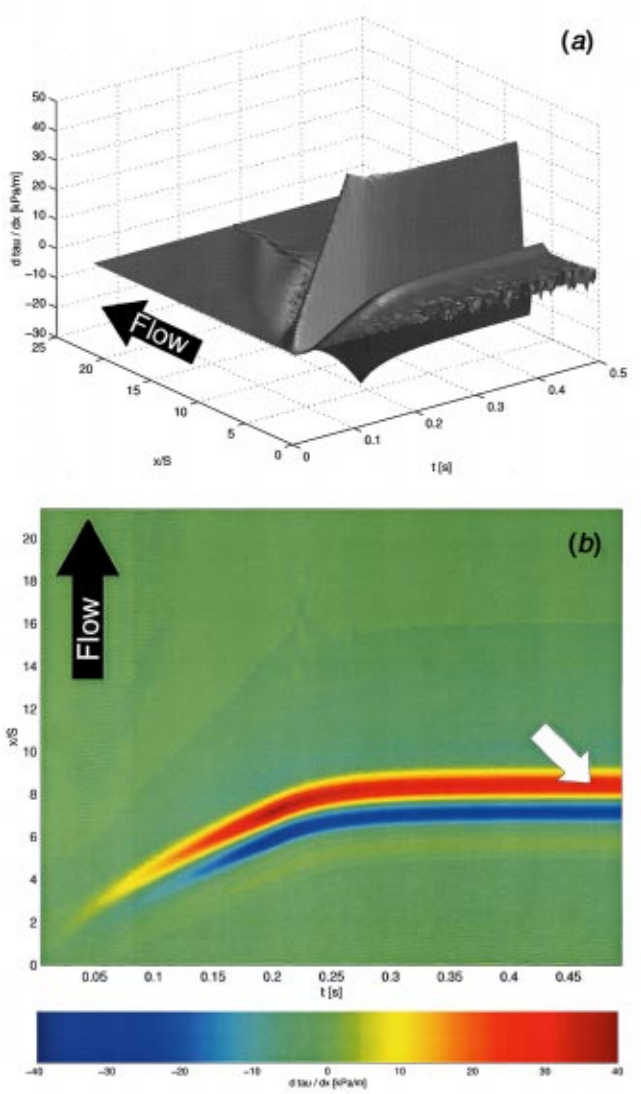

Fig. 7 Spatial partial derivative of the function shown in Fig. 5. As in Fig. 5, the same data are presented as a three-dimensional graph and a two-dimensional false-color contour plot. It can be seen that the zone with the highest spatial gradients matches the second stagnation point. At the end of the ramping period, a maximum spatial gradient can be observed that is slightly higher than the steady-state gradient. As opposed to the temporal gradients, the spatial gradients do not vanish when the system reaches equilibrium.

vivo conditions, the cells were not subjected to shear stress prior to the experiment. Although preconditioning of cells to shear stress may be considered more physiological [24], most studies analyzing shear stress patterns do not apply shear stress prior to the experiment, and there is no evidence that the response of the cells would be qualitatively different for the purpose of comparing the effects of temporal and spatial gradients.

In recirculation zones, sites of low mean flow, high spatial gradients, and high temporal gradients coincide. The established model for disturbed arterial flow, the backward-facing step chamber, also superimposes these three putative stimuli. Since previously the characteristics of the spatial gradients have been extensively reported upon [7,8,14,16], this study analyzes the temporal dynamics of shear stress in the model. In order to obtain a clear response of the cells, both temporal and spatial gradients were chosen to be relatively high. Given the nature of the shear stress profile, however, a broad range of shear stress values is covered

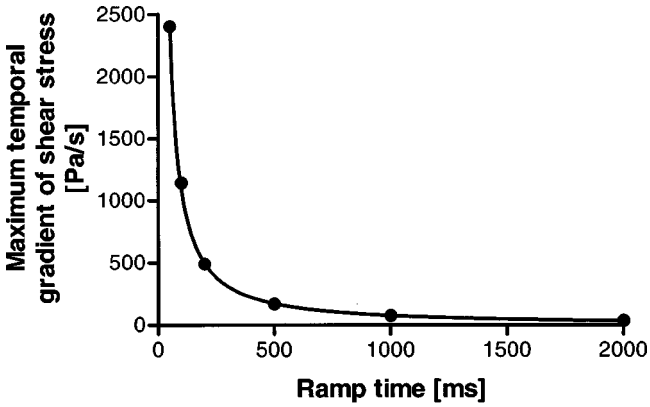

Fig. 8 The maximum temporal gradient of shear stress as a function of the ramp time. The data points were computed for the discrete ramp times 50, 100, 200, 500 ms and 1, 2, and 15 s. Due to scaling reasons, the 15 s data point is not shown. A nonlinear curve fit shows that the data points are well represented by the function $\dot{\tau}_{max}=A\cdot t_{ramp}^{-B}$ with $A=221.5$ and $B=1.15$ ($R^2=0.999$). With $t_{ramp}\rightarrow\infty$ the temporal gradient $\dot{\tau}$ vanishes.

depending on the position of the cells downstream from the sudden expansion point. In the region from $x=6.6$ to 7.7 mm, significantly higher cell proliferation rates were observed for $t_{ramp}=200$ ms (35.5 Pa/s) than in the slowly ramped case, $t_{ramp}=15$ s. Similarly, the recirculating flow pattern also subjected cells to a large range of spatial gradients (0–40 kPa/m in the case of ramped flow), which included levels that have been measured in vivo [25]. In ramp flow, this entire range of spatial gradients failed to stimulate proliferation.

Consistent with previous studies of endothelial proliferation in regions of recirculating flow [8,14,26], a sudden onset of flow in the backward-facing step model lead to a significant stimulation of endothelial cell proliferation in a region close to the second stagnation point (Fig. 11). As Fig. 12 shows, the increased proliferation rate at sudden onset of flow relative to the proliferation

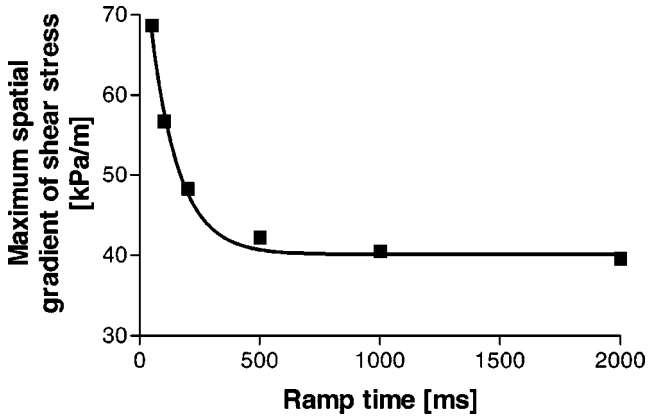

Fig. 9 The maximum spatial gradient of shear stress as a function of the ramp time. The data points were computed for the same discrete ramp times as in Fig. 8. A good fit can be achieved with an exponential decay function, $\tau'_{max}=s\cdot\exp(-t_{ramp}/K_t)+P$ with the constants $s=42.7$ kPa/m, $K_t=8.6$ ms, and $P=40.11$ kPa/m and a regression coefficient of $R=0.996$. As opposed to temporal gradients of shear stress, spatial gradients do not vanish with slow ramping times, but rather approach a lower boundary. Also, the increase of spatial gradients with shorter ramp times is by orders of magnitude less pronounced than in the case of temporal gradients.

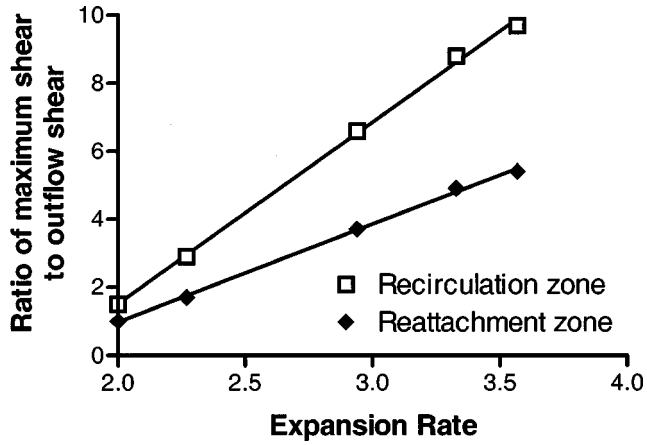

Fig. 10 Dependency of the maximum shear stress in the recirculation zone (□) and the forward reattachment zone (♦) on the expansion ratio. A high expansion ratio leads to an amplification of the maxima relative to the outflow shear stress.

rate at ramped onset match the spatial distribution of exposure to temporal shear stress gradients. In our experiments, we calculated maximum spatial gradients of 39 kPa/m for the ramped onset and 48 kPa/m for the sudden onset. The higher value in the sudden-onset experiment persists only for a short time at $t \approx t_{ramp}$. Thus, the difference is approximately 23 percent. In other studies, cell activation has been reported at spatial gradient values of less than 7 kPa/m [7,8]. It is therefore conceivable that the stimulus of 40 kPa/m and more saturates the mechanism and the 23 percent difference may be considered minor. On the other hand, the highest temporal gradient is about 300 times higher in the sudden-onset case than in the slowly ramped case. Although the duration of the exposure to temporal gradients of shear stress is very short in comparison to the total duration of flow exposure, our results suggest that it has a strong and localized stimulatory effect on endothelial proliferation. In support of the observation of a mitogenic effect of temporal gradients, Bao and co-workers [11] have shown that temporal changes as short as 3 seconds can stimulate

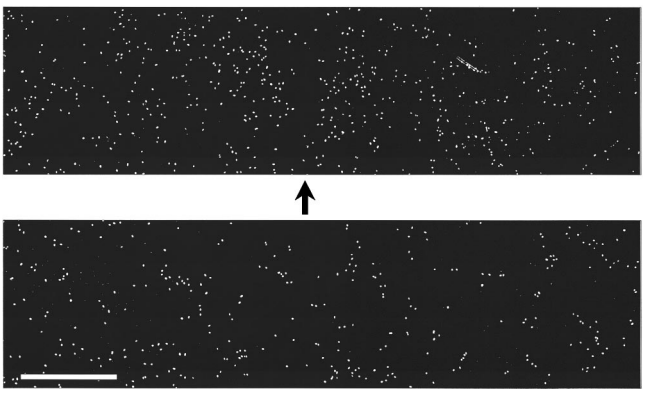

Fig. 11 Immunofluorescent micrographs of BrdU positive nuclei after 4 h exposure to recirculating flow in the backward-facing step chamber. Shown is a representative example from a paired set of HUVEC slides with cells exposed to a sudden onset of flow in the upper panel, and cells exposed to ramped flow (15 s) below. Each micrograph is a photo-construct that comprises three contiguous HPF. Micrographs span the region of flow recirculation and reattachment (2.2 mm to 9.0 mm downstream from the expansion site). The white dots represent BrdU positive proliferating nuclei. The scaling bar equals 1.1 mm, and the arrow indicates the position of the second stagnation point.

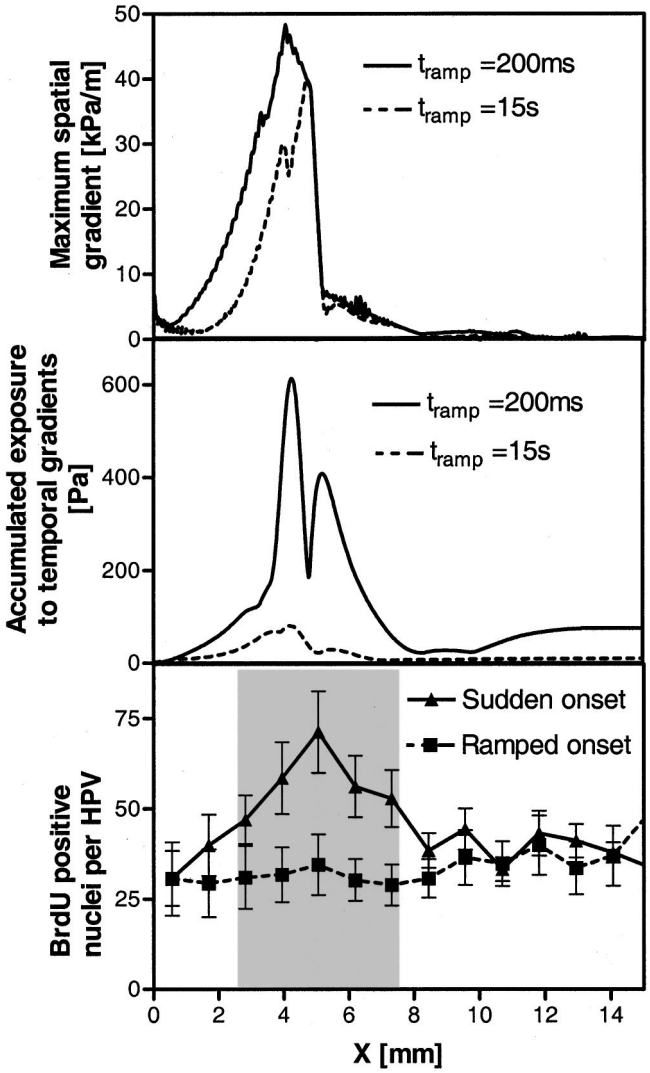

Fig. 12 Cell exposure to temporal gradients compared to cell proliferation rate. Shown is the cell proliferation of cells exposed to shear stress at sudden onset of flow (200 ms, –▲–) relative to the proliferation rate for ramped (15 s) onset of flow (–■–) [27], lower panel. The difference between cell proliferation rates with sudden and ramped onset of flow are statistically significant within the fields of view from 2.25 to 7.88 mm (shaded area). The total exposure of the cells to temporal shear stress gradients is shown in the middle panel for sudden onset of flow (solid line) versus ramped onset of flow (dashed line). Similarly, the maximum exposure of the cells to spatial gradients is shown in the upper panel for both flow conditions.

increasing and sustained expression of several pro-mitogenic factors four hours after initial exposure to a short impulse of flow. A more extensive study was targeted directly at the cellular response to defined and isolated spatial and temporal gradients of shear stress [27]. In a backward-facing step chamber, a sudden onset of flow stimulated endothelial cell proliferation twofold compared to a ramped onset of flow. In a parallel-plate flow chamber, a single 500 ms impulse of shear stress (1 Pa) led to 50 percent higher cell proliferation than both sham control and cells exposed to slowly ramped flow. These results demonstrate that endothelial cells are sensitive to very short transient stimulation events, while the absence of temporal gradients fail to stimulate proliferation, even if high spatial gradients are present.

The fact that the recirculation zone in a backward-facing step flow chamber does not develop instantaneously with an instantaneous onset of flow but needs a sub-second time to reach a steady state from the initial condition $u(x, y) = 0$ for all x, y within the

flow domain was reported by Durst and Pereira [15]. In this study, the same established algorithms [15,28] have been employed to simulate variable onset phases of flow numerically in a backward-facing step flow chamber and to obtain quantitative values of the shear stresses and the temporal gradients thereof that the cells are exposed to. To understand better the influence of spatial and temporal gradients of shear stress, the characterization of the temporal behavior of fluid flow in the backward-facing step flow chamber is of fundamental importance. Flow conditions likely to be found in experimental apparatus were simulated, as determined by flow visualization. The Reynolds numbers used were close to those occurring in major arteries [29]. In the model, flow onset was assumed to follow a linear increase from a very low flow rate to its final flow rate within a variable ramp time. By varying this ramp time, the exposure of the cells to temporal gradients can be modulated. Figure 8 shows the dependency of the highest temporal shear stress gradient on the time of flow onset. Empirically, a hyperbolical relationship $\dot{\tau} \propto t_{\text{ramp}}^{-B}$ was calculated by nonlinear regression. This relationship is provided as a quick means to determine the maximum temporal gradients occurring at a specific flow condition. However, this empirical relationship has a tendency to overestimate the magnitude of the temporal gradient at high ramp times and should therefore only be used as a rough estimate. Spatial gradients of shear stress also exhibit a dynamic behavior. A transient maximum of the spatial gradient can be observed at the end of the ramping period (Fig. 7), where the height depends on the ramp time. While the two cases presented here (sudden onset, 200 ms, 488 Pa/s, and slowly ramped onset, 15 s, 1.66 Pa/s) differ by a factor of 300 in the magnitude of temporal gradients, there is merely 23 percent difference in spatial gradients. Furthermore, spatial gradients do not vanish with long ramp times. Congruously, very long ramp times lead to negligible temporal gradients, while spatial gradients persist. Thus, the backward-facing step flow chamber allows the exposure to spatial gradients alone, or to a combination of temporal and spatial gradients. A parallel-plate flow chamber [18] with its undisturbed flow regime does not generate spatial gradients (with the exception of a short entrance length of 0.2 mm [18]). Thus, cells sheared in a parallel-plate flow chamber will be exposed to temporal gradients alone. The same applies to the outflow region far downstream from the expansion site (in the presented case, $X/S > 30$) in a sudden-expansion flow chamber.

Under the assumption of a 200 ms onset phase, the time found to correspond to the sudden onset of flow in the experimental apparatus, the temporal gradient in the region of fully re-established flow is 5.6 Pa/s as opposed to approximately 330 Pa/s in the forward reattachment zone and 490 Pa/s in the recirculation zone (Fig. 10). The geometry of the backward-facing step leads to a local amplification of the shear stress in small zones upstream and downstream of the second stagnation point. For the flow chamber described by Chiu et al. [7], the expansion ratio was 1:2, which generates a very moderate local amplification in the recirculation zone. The flow chamber described by Truskey et al. [14] with its expansion ratio of 1:2.37 shows a significantly higher local amplification: Maximum shear stress in the recirculation zone is about three times higher than the outflow shear stress. The geometry of the backward-facing step flow chamber used in this study had an expansion ratio of 1:3.4, which led to a local amplification ratio of more than 8, leading to very high temporal and spatial gradients of shear stress. The physiological relevance varies from arterial bifurcations to stenoses, where diameter reductions of up to 70 percent (expansion ratio 1:3.3) can occur [7,29–31]. The results presented in this study allow an estimate of the shear stress properties the cells will be exposed to under a given geometry and flow rate.

In summary, we have shown that in a backward-facing step flow chamber, cells are exposed to both temporal and spatial gradients of shear stress. Depending on the flow onset time (ramp time), the temporal gradients cause a significant mitogenic response in endothelial cells, which are related to observations at sites of disturbed flow in the vascular endothelium.

Acknowledgments

We thank Dr. Nicolas L'Heureux for many helpful thoughts and for his video visualizations of the flow. This study was supported by National Heart, Lung and Blood Institute Grant: No. HL-40696. Haidekker and White are recipients of National Research Service Award fellowships from the National Institute of Health, Nos. 1F32GM20476-01 and 1F32HL10370-01.

Nomenclature

- A = constant (curve fit)
- B = constant (curve fit)
- F = tentative flow field $F(x, y)$ used in the numerical scheme
- g = body forces
- H = channel height, particularly for a parallel-plate flow chamber
- K_t = constant (curve fit)
- L = inflow channel height
- t = time
- t_{ramp} = ramp time, time over which the flow velocity is linearly increased before reaching a constant level
- P = constant (curve fit)
- p = pressure field $p(x, y)$
- Q = average flow rate
- Q_{max} = maximum average flow rate which is held constant at $t > t_{\text{ramp}}$
- Re = Reynolds number
- S = step height
- s = constant (curve fit)
- u = velocity field $u(x, y)$ comprising the components u_x and u_y
- u_∞ = average medium velocity at inflow
- w = channel depth (extension perpendicular to both x and y)
- x = coordinate axis, distance from the sudden-expansion point
- y = coordinate axis
- μ = dynamic viscosity of the medium
- ρ = density of the medium
- τ = shear stress (general)
- τ_w = wall shear stress for Poiseuille flow
- τ_∞ = wall shear stress in the reattached region, sufficiently downstream from the second stagnation point
- $\dot{\tau}$ = temporal gradient of shear stress, partial derivative of τ with respect to time
- τ' = spatial gradient of shear stress, partial derivative of τ with respect to the distance from the sudden-expansion point x
- κ = factor used in the computation of the discrete time steps

Appendix

The algorithm used for the time-dependent numerical simulations has been described in [28]. In this algorithm, the momentum equation is discretized in time using the Euler method, which results in:

$$u^{(n+1)} = u^{(n)} + \delta t \left[\frac{1}{\text{Re}} \Delta u^{(n)} - (u^{(n)} \,\text{grad}) u^{(n)} - \text{grad}\, p^{(n)} + g \right] \tag{11}$$

The time-stepping loop comprises the following steps:

1 Setup of the geometry-dependent boundary conditions.

2 Initialize the velocity field $u=(u_x,u_y)$ and the pressure field p. In this study, a steady-state result from a previous calculation with the same geometry and Re=10 was used.
3 Repeat steps 4 to 8 from $t=0$ to t_{end},
4 Calculate a new δt that satisfies the stability condition (4). Also, calculate the new Reynolds number for the given time if the flow is to be ramped.
5 Calculate a tentative velocity field $F=(F_x,F_y)$ using Eq. (12), which is independent of the pressure:

$$F^{(n)}=u^{(n)}+\delta t\left[\frac{1}{\text{Re}}\Delta u-(u\nabla)u+g\right] \tag{12}$$

6 For the tentative velocity, iteratively solve the Poisson Eq. (13) using the Gauss–Seidel method with successive overrelaxation:

$$\Delta p^{(n)}=\frac{1}{\delta t}\nabla F^{(n)} \tag{13}$$

7 Calculate the final velocity field by adding the pressure term to the tentative velocity according to Eq. (14):

$$u^{(n+1)}=F^{(n)}+\delta t\,\text{grad}\,p^{(n)} \tag{14}$$

8 Adjust the boundary conditions for pressure and velocity to reflect no-slip-conditions on the walls and $\partial u_x/\partial x=0$ at the outflow. Calculate the bottom plate shear stress using Eq. (15):

$$\tau(x,t)=\mu\left.\frac{\partial u_x(x,t)}{\partial y}\right|_{y=0} \tag{15}$$

References

[1] Glagov, S., Zarins, C., Giddens, D. P., and Ku, D. N., 1988, ''Hemodynamics and Atherosclerosis. Insights and Perspectives Gained From Studies of Human Arteries,'' Arch. Pathol. Lab. Med., **112**, pp. 1018–1031.
[2] Davies, P. F., Barbee, K. A., Volin, M. V., Robotewskyj, A., Chen, J., Joseph, L., Griem, M. L., Wernick, M. N., Jacobs, E., Polacek, D. C., Depaola, N., and Barakat, A. I., 1999, ''Spatial Relationships in Early Signaling Events of Flow-Mediated Endothelial Mechanotransduction,'' Annu. Rev. Physiol., **59**, pp. 527–549.
[3] Davies, P. F., Polacek, D. C., Handen, J. S., Helmke, B. P., and Depaola, N., 1999, ''A Spatial Approach to Transcriptional Profiling: Mechanotransduction and the Focal Origin of Atherosclerosis,'' Trends Biotechnol., **17**, pp. 347–351.
[4] Kuchan, M. J., and Frangos, J. A., 1994, ''Role of Calcium and Calmodulin in Flow-Induced Nitric Oxide Production in Endothelial Cells,'' Am. J. Physiol., **266**, pp. C628–C636.
[5] Frangos, J. A., Eskin, S. G., Mcintire, L. V., and Ives, C. L., 1985, ''Flow Effects on Prostacyclin Production by Cultured Human Endothelial Cells,'' Science, **227**, pp. 1477–1479.
[6] Levesque, M. J., Nerem, R. M., and Sprague, E. A., 1990, ''Vascular Endothelial Cell Proliferation in Culture and the Influence of Flow,'' Biomaterials, **11**, pp. 702–707.
[7] Chiu, J. J., Wang, D. L., Chien, S., Skalak, R., and Usami, S., 1998, ''Effects of Disturbed Flow on Endothelial Cells,'' ASME J. Biomech. Eng., **120**, pp. 2–8.
[8] Depaola, N., Gimbrone, M. A., Jr., Davies, P. F., and Dewey, C. F., Jr., 1992, ''Vascular Endothelium Responds to Fluid Shear Stress Gradients,'' Arterioscler. Thromb., **12**, pp. 1254–1257.
[9] Ojha, M., 1994, ''Wall Shear Stress Temporal Gradient and Anastomotic Intimal Hyperplasia,'' Circ. Res., **74**, pp. 1227–1231.
[10] Ku, D. N., Giddens, D. P., Zarins, C. K., and Glagov, S., 1985, ''Pulsatile Flow and Atherosclerosis in the Human Carotid Bifurcation. Positive Correlation Between Plaque Location and Low Oscillating Shear Stress,'' Arteriosclerosis **5**, 293–302.
[11] Bao, X., Lu, C., and Frangos, J. A., 1999, ''Temporal Gradient in Shear but Not Steady Shear Stress Induces PDGF-A and MCP-1 Expression in Endothelial Cells: Role of NO, NF Kappa B, and Egr-1,'' Arterioscler., Thromb., Vasc. Biol., **19**, pp. 996–1003.
[12] Bao, X., Clark, C. B., and Frangos, J. A., 2000, ''Temporal Gradient in Shear-Induced Signaling Pathway: Involvement of MAP Kinase, C-Fos, and Connexin43,'' Am. J. Physiol., **278**, pp. H1598–H1605.
[13] Moore, J. E., Jr., Xu, C., Glagov, S., Zarins, C. K., and Ku, D. N., 1994, ''Fluid Wall Shear Stress Measurements in a Model of the Human Abdominal Aorta: Oscillatory Behavior and Relationship to Atherosclerosis,'' Atherosclerosis, **110**, pp. 225–240.
[14] Truskey, G. A., Barber, K. M., Robey, T. C., Olivier, L. A., and Combs, M. P., 1995, ''Characterization of a Sudden Expansion Flow Chamber to Study the Response of Endothelium to Flow Recirculation,'' ASME J. Biomech. Eng., **117**, pp. 203–210.
[15] Durst, F., and Pereira, J. C. F., 1988, ''Time-Dependent Laminar Backward-Facing Step Flow in a Two-Dimensional Duct,'' ASME J. Fluids Eng., **110**, pp. 289–296.
[16] Armaly, B. F., Durst, F., Pereira, J. C. F., and Schönung, B., 1982, ''Experimental and Theoretical Investigation of Backward-Facing Step-Flow,'' J. Fluid Mech., **127**, pp. 473–496.
[17] Kaiktsis, L., Karniadakis, G. E., and Orszag, S. A., 1991, ''Onset of Three-Dimensionality, Equilibria, and Early Transition in Flow Over a Backward-Facing Step,'' J. Fluid Mech., **231**, pp. 501–528.
[18] Frangos, J. A., Mcintire, L. V., and Eskin, S. G., 1988, ''Shear Stress Induced Stimulation of Mammlian Cell Metabolism,'' Biotechnol. Bioeng., **32**, pp. 1053–1060.
[19] White, C. W., Haidekker, M. A., and Frangos, J. A., 2001, ''Temporal Gradients in Shear, but Not Spatial Gradients, Stimulate Endothelial Cell Proliferation,'' Circulation, **103**, pp. 2508–2513.
[20] Wright, H. P., 1972, ''Mitosis Patterns in Aortic Endothelium,'' Atherosclerosis, **15**, pp. 93–100.
[21] Depaola, N., Davies, P. F., Pritchard, W. F., Jr., Florez, L., Harbeck, N., and Polacek, D. C., 1999, ''Spatial and Temporal Regulation of Gap Junction Connexin43 in Vascular Endothelial Cells Exposed to Controlled Disturbed Flows in Vitro,'' Proc. Natl. Acad. Sci. U.S.A., **96**, pp. 3154–3159.
[22] Nagel, T., Resnick, N., Dewey, C. F., Jr., and Gimbrone, Jr., M. A., 1999, ''Vascular Endothelial Cells Respond to Spatial Gradients in Fluid Shear Stress by Enhanced Activation of Transcription Factors,'' Arterioscler., Thromb., Vasc. Biol., **19**, pp. 1825–1834.
[23] Long, Q., Xu, X. Y., Ariff, B., Thom, S. A., Hughes, A. D., and Stanton, A. V., 2000, ''Reconstruction of Blood Flow Patterns in a Human Carotid Bifurcation: a Combined CFD and MRI Study,'' J. Magn. Reson Imaging, **11**, pp. 299–311.
[24] Pedersen, E. M., Agerbaek, M., Kristensen, I. B., and Yoganathan, A. P., 1997, ''Wall Shear Stress and Early Atherosclerotic Lesions in the Abdominal Aorta in Young Adults,'' Eur. J. Vasc. Endovasc Surg., **13**, pp. 443–451.
[25] Ziegler, T., and Nerem, R. M., 1994, ''Effect of Flow on the Process of Endothelial Cell Division,'' Arterioscler. Thromb., **14**, pp. 636–643.
[26] Lutz, R. J., Cannon, J. N., Bischoff, K. B., Dedrick, R. L., Stiles, R. K., and Fry, D. L., 1977, ''Wall Shear Stress Distribution in a Model Canine Artery During Steady Flow,'' Circ. Res., **41**, pp. 391–399.
[27] Tardy, Y., Resnick, N., Nagel, T., Gimbrone, Jr., M. A., and Dewey, C. F. Jr., 1997, ''Shear Stress Gradients Remodel Endothelial Monolayers in Vitro Via a Cell Proliferation-Migration-Loss Cycle,'' Arterioscler., Thromb., Vasc. Biol., **17**, pp. 3102–3106.
[28] Griebel, M., Dornseifer, T., and Neunhoeffer, T., 1998, ''Numerical Simulations in Fluid Dynamics,'' SIAM, Philadelphia.
[29] Young, D. F., 1979, ''Fluid Mechanics of Arterial Stenoses,'' ASME J. Biomech. Eng., **101**, pp. 157–175.
[30] Calvo, W. J., Hajduczok, G., Russell, J. A., and Diamond, S. L., 1999, ''Inhibition of Nitric Oxide but Not Prostacyclin Prevents Poststenotic Dilatation in Rabbit Femoral Artery,'' Circulation, **99**, pp. 1069–1076.
[31] Yongchareon, W., and Young, D. F., 1979, ''Initiation of Turbulence in Models of Arterial Stenoses,'' J. Biomech., **12**, pp. 185–196.